Beryllium sites in MBE-grown BeZnO alloy films

2014 J. Phys. D: Appl. Phys. 47 175102

(http://iopscience.iop.org/0022-3727/47/17/175102)

IOP Publishing Journal of Physics D: Applied Physics
J. Phys. D: Appl. Phys. **47** (2014) 175102 (6pp) doi:10.1088/0022-3727/47/17/175102

Beryllium sites in MBE-grown BeZnO alloy films

Daqian Ye[1], Zengxia Mei[1,3], Huili Liang[1], Yulong Liu[1], Alexander Azarov[2], Andrej Kuznetsov[2] and Xiaolong Du[1,3]

[1] Key Laboratory for Renewable Energy, Beijing National Laboratory for Condensed Matter Physics, Institute of Physics, Chinese Academy of Sciences, Beijing, 100190, People's Republic of China
[2] Department of Physics, University of Oslo, Oslo, N-0316, Norway

E-mail: zxmei@iphy.ac.cn (Z Mei) and xldu@iphy.ac.cn (X Du)

Received 22 March 2014, revised 22 February 2014
Accepted for publication 10 March 2014
Published 10 April 2014

Abstract

We report the possible sites that beryllium atoms can occupy in BeZnO alloy films by a comparative study. The epitaxial $Be_xZn_{1-x}O$ ($x = 0, 0.06, 0.1, 1$) films were prepared by a molecular beam epitaxy technique, and their structural properties were characterized with x-ray diffraction, Raman spectroscopy and x-ray photoelectron spectroscopy, while the Be composition, x, was measured with time of flight elastic recoil detection analysis. When x is 6%, substitutional and interstitial Be atoms are revealed to be co-existing in $Be_xZn_{1-x}O$ films. Furthermore, phase segregation of BeO is observed when x increases to 10% due to the huge difference of the bond length between Be–O and Zn–O. In this case, most of the Be atoms are found to form BeO particles, rather than a BeZnO alloy, so as to reduce the formation energy. The incorporation of Be atoms in the ZnO lattice consequently decreases in $Be_{0.1}Zn_{0.9}O$, resulting in a smaller bandgap than that of $Be_{0.06}Zn_{0.94}O$.

Keywords: BeZnO, interstitial, phase segregation, x-ray photoelectron spectroscopy, Raman, molecular beam epitaxy, time-of-flight elastic recoil detection analysis

(Some figures may appear in colour only in the online journal)

As an alloy of BeO and ZnO, BeZnO has been considered to be a promising candidate for applications in short-wavelength light-emitting devices and photodetectors (PDs) [1, 2]. One of its unique advantages is the theoretically tunable wide bandgap from 3.37 eV (ZnO) to 10.6 eV (BeO), which is quite important for use alone or in combination to form active layers and devices that can emit and detect one or a multiplicity of wavelengths over a wide range of wavelengths. Actually, one of its congeneric semiconductors, $Mg_xZn_{1-x}O$, has been widely investigated in recent decades, for its possibly tuned bandgap in the large range from 3.37 to 7.8 eV (MgO). Due to the huge discrepancy in lattice structure between ZnO (wurtzite with a lattice constant of $a = 3.25$ Å, $c = 5.20$ Å) and MgO (rock salt with a lattice constant of 4.22 Å), wurtzite $Mg_xZn_{1-x}O$ (W-$Mg_xZn_{1-x}O$) with a high Mg content or cubic $Mg_xZn_{1-x}O$ (C-$Mg_xZn_{1-x}O$) with a high Zn content (namely low Mg content) tend to separate into wurtzite ZnO and cubic MgO mixtures during the growth, known as phase segregation. This problem may be hopefully suppressed by delicately controlling the growth conditions, resulting in a shift into the deeper ultraviolet (UV) band [3, 4]. The highest Mg content ever reported is 55%, and solar-blind UV PDs based on this material have been realized with a sharp cutoff wavelength at 270 nm [5, 6]. The common phase segregation problem in MgZnO seems to be not a big challenge for BeZnO, since BeO has the same hexagonal wurtzite structure as ZnO. In this case, the bandgap of BeZnO is expected to be easily modulated into the deep UV region, with a much smaller Be composition in contrast to Mg. It has been reported that $Be_xZn_{1-x}O$ films could be deposited with a bandgap ranging from 3.37 to 10.6 eV by using hybrid beam deposition, where no phase segregation between ZnO and BeO was detected in the BeZnO alloy [7]. However, some results indicate that the energy band gap of the $Be_xZn_{1-x}O$ layer cannot be tuned so flexibly in a wide range as expected even when the Be composition of x reaches 11% [8].

[3] Authors to whom any correspondence should be addressed.

More importantly, it has been predicted that Be–N bonds in ZnO are shallow acceptor levels by preliminary band-structure calculations of ZnO containing metal–N bonds [9]. It was expected that N-related deep acceptor levels could be greatly modified due to the stronger bonding of Be–N than Zn–N, resulting in an effective p–ZnO [10, 11]. However, the Hall-effect measurement results suggest that high-resistant films were obtained. Recently, a first-principles calculation result indicates that Be atoms tend to be in the interstitial sites (Be_i), considering the large difference of ionic radius between Be^{2+} (0.27 Å) and Zn^{2+} (0.60 Å) [12]. The calculation shows that the formation of a complex defect of $4Be_{Zn}$–N_O, that is, four substitutional Be atoms at the Zn site (Be_{Zn}) and one substitutional N atom at the O site (N_O), is very difficult, based on the high formation energy (1.95 eV), while the complex of Be_i–$2N_O$ (one interstitial Be atom and two substitutional N atoms at O site) is a neutral complex that stably exists in co-doped ZnO due to the Coulomb attraction. If the hypotheses are correct, it's also quite reasonable why the bandgap and electrical properties of $Be_xZn_{1-x}O$ cannot be readily modulated. On the other hand, the phase segregation problem of $Zn_xBe_{1-x}O$, i.e., Zn-doped BeO, has been seldom valued. These two issues need to be clarified regarding their significant impacts on bandgap engineering and the p-type doping of $Be_xZn_{1-x}O$.

In this paper, the possible sites of Be in BeZnO alloy films are comparatively investigated. The BeZnO films were synthesized on an α-Al_2O_3(0 0 0 1) substrate by radio-frequency plasma assisted molecular beam epitaxy (RF-MBE) with a base pressure of 1×10^{-7} Pa. Elemental Be (4 N) and Zn (7 N) evaporated by Knudsen cells (Veeco), and radical oxygen generated by an RF-plasma system (SVTA), were used as sources for the growth. The substrate was cleaned with acetone and ethanol for 5 min, and then was rinsed in deionized water. After being loaded into the chamber, the substrate was heated up to 750 °C for thermal cleaning and was subsequently exposed to oxygen plasma at 500 °C in order to obtain a uniform oxygen-terminated surface. An unrelaxed cubic MgO ultrathin layer (~2 nm) was chosen to modify the complex α-Al_2O_3(0 0 0 1) surface structure, as reported in our previous study [13]. It has been proved that the ultrathin MgO interfacial layer is very critical for unipolar wurtzite $Mg_xZn_{1-x}O$ growth on sapphire, which is also suitable for BeZnO films. To investigate the alloying behaviour of Be in ZnO, $Be_xZn_{1-x}O$ epilayers with $x = 0$, 0.06, 0.1 and 1 were prepared separately. The Zn cell was kept at 315 °C, and the temperature of the Be cell increased from 0 °C, 890 °C, 950 °C and 1050 °C, corresponding to the samples of ZnO, $Be_{0.06}Zn_{0.94}O$, $Be_{0.1}Zn_{0.9}O$ and BeO, respectively. Growth of the BeO film by the same method is very important, because it can provide more solid evidence of our conclusions. The thicknesses of the $Be_xZn_{1-x}O$ films reported here were around 150 nm.

The whole growth process was *in situ* monitored by reflection high-energy electron diffraction (RHEED), where the evolution of crystal structures and qualities can be clearly seen. The crystal structures of the epilayers were further investigated by *ex situ* x-ray diffraction (XRD) measurements. Be compositions were confirmed by a time-of-flight elastic recoil detection analysis (ToF-ERDA) technique. X-ray photoelectron spectroscopy (XPS, PHI Quantera SXM, Al Kα source: $h\nu = 1486.6$ eV) was applied to detect the valence states of Be in the films. In XPS spectroscopy, the binding energies were calibrated by taking the carbon C1s peak (284.8 eV) as a reference. The optical bandgap was characterized by the reflectance spectrum (RS) carried out at room temperature. The electrical properties were measured in a homemade automatic four-probe Hall measurement system with a Van der Pauw configuration. For the four-probe Hall measurement, the constant current I was supplied by a programmable dc source (Keithley 2400), and the corresponding voltage drop V between contacts was measured using a high-impedance, high-resolution voltmeter (Keithley 2000). They were controlled by a computer through a GPIB bus with the IEEE 488 protocol. The magnetic field was generated by employing an electromagnet with a computer-controlled current source. The results were calculated by tracing Hall voltage curves, which can tell an accurate carrier type and mobility. To investigate the difference of lattice stains caused by different Be compositions, Raman spectra were measured in the range of 50–1100 cm^{-1} using the 532 nm excitation lines from a Nd^{3+} : YAG laser on a LabRam HR-800 spectrometer.

Shown in figure 1(*a*) are the RHEED patterns of ZnO, BeO, $Be_{0.06}Zn_{0.94}O$ and $Be_{0.1}Zn_{0.9}O$, respectively. The six-fold symmetry is observed in all of the samples, indicating they all have the single wurtzite structure. It should be noted that the reciprocal rods of the BeO layer have a larger space compared to that of ZnO. That is because the in-plane lattice constant of BeO ($a = 2.699$ Å) is smaller than that of ZnO ($a = 3.249$ Å). In the case of $Be_{0.06}Zn_{0.94}O$ and $Be_{0.1}Zn_{0.9}O$, on the other hand, the reciprocal spacing changes not so much, which is reasonable considering the small number of Be atoms incorporated. The diffraction spots in $Be_{0.1}Zn_{0.9}O$ are bigger and more dispersive, indicating a worse crystal quality. More Be incorporation will result in a notable phase segregation and even polycrystals (not shown here).

Determination of the accurate Be compositions in $Be_xZn_{1-x}O$ alloys was performed by ToF-ERDA in our experiments. Based on the detection of atoms that are knocked out from the sample by the incoming heavy ions, iodine (^{127}I), ToF-ERDA is a powerful tool to accurately distinguish the lighter elements such as H, He and Be [14]. In short, the kinetic energies of the atoms (E) as well as their time-of-flight (t_{ToF}) within a certain distance (L) are measured, and the $t_{ToF} = L\sqrt{m/2E}$, so the mass of the flying atoms, m, can be extracted by t_{ToF}–E plot. Figures 1 (*b*) and (*c*) show the ToF-ERDA spectra of $Be_{0.06}Zn_{0.94}O$ and $Be_{0.1}Zn_{0.9}O$ samples. It can be seen that different chemical elements are represented by different distributions of concentrated dots. All the elements were identified and labelled accordingly, including Al and O from the substrate as well as Zn, Be and O in the film. The bottom rows of figures 1 (*b*) and (*c*) are the depth profiles of all elements in $Be_{0.06}Zn_{0.94}O$ and $Be_{0.1}Zn_{0.9}O$, respectively. It should be noticed that Be and Zn concentrations are basically uniform within a depth of at least 100 nm inside the epilayers.

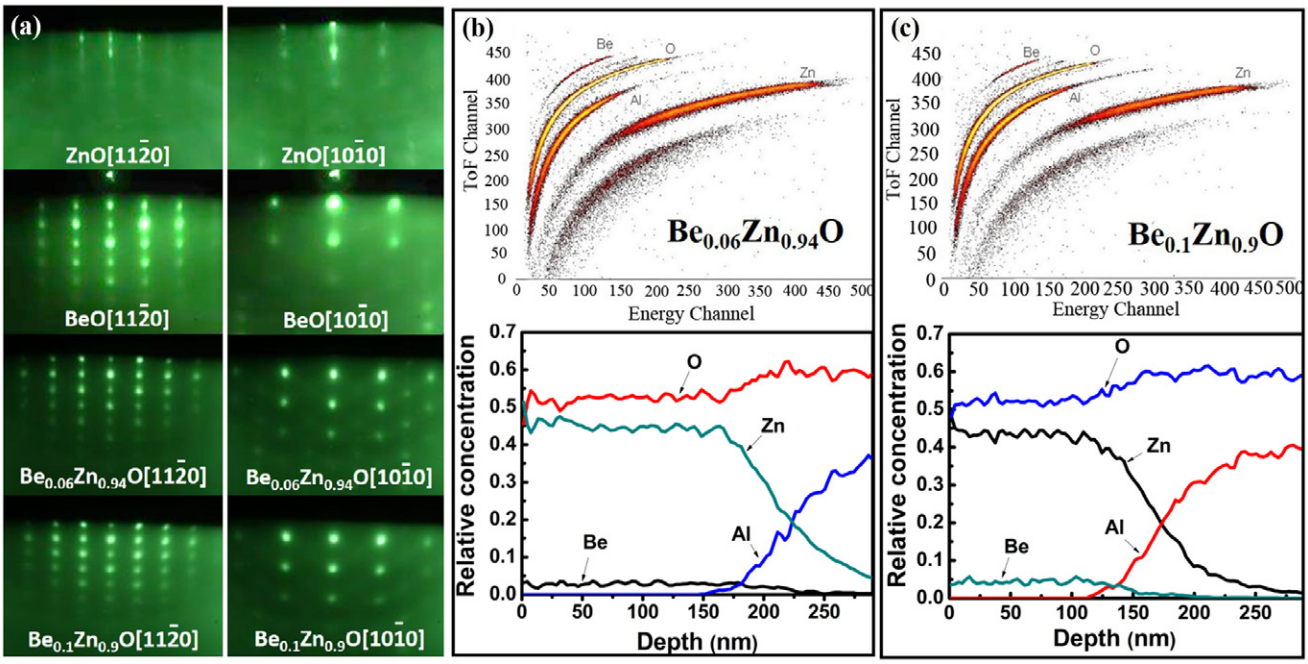

Figure 1. (*a*) RHEED patterns of ZnO, BeO, $Be_{0.06}Zn_{0.94}O$ and $Be_{0.1}Zn_{0.9}O$ films, respectively. ToF-ERDA spectra and extracted element depth profiles in Be_xZnO_{1-x} films with $x = 0.06$ (*b*) and $x = 0.1$ (*c*).

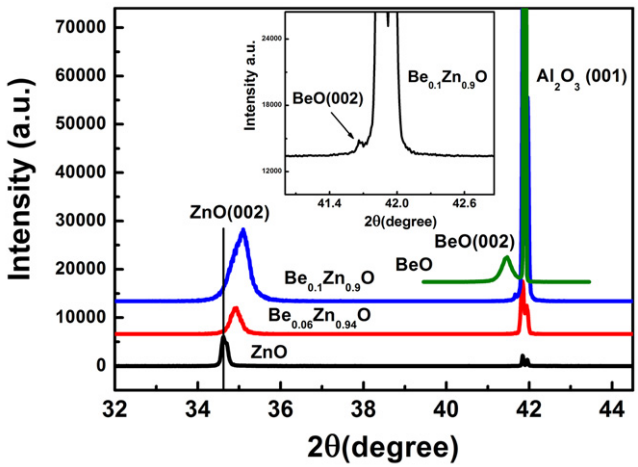

Figure 2. XRD θ–2θ scan results of ZnO, BeO, $Be_{0.06}Zn_{0.94}O$ and $Be_{0.1}Zn_{0.9}O$ films. The inset shows the enlarged curve of $Be_{0.1}Zn_{0.9}O$ in the 2θ range from 41° to 43°. The intensity of ZnO has been divided by five for a better comparison.

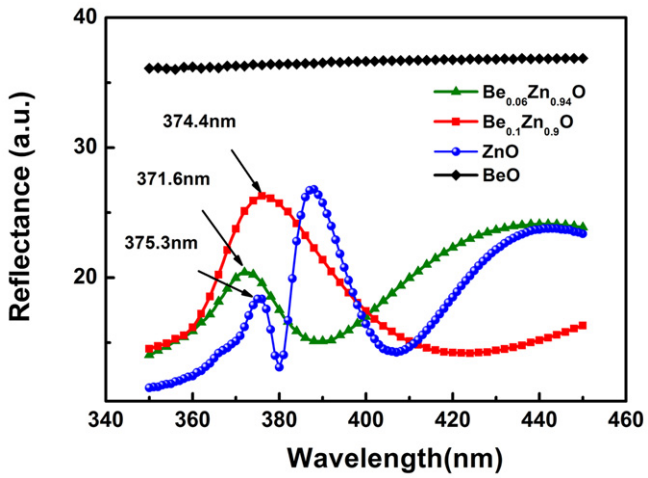

Figure 3. Reflectance spectra of ZnO, BeO, $Be_{0.06}Zn_{0.94}O$ and $Be_{0.1}Zn_{0.9}O$ films, respectively. The intensity of BeO reflectance has been divided by two for a better view.

In this region, the Be concentrations are determined as 6% and 10%, respectively.

To confirm the single wurtzite crystal structure of the epilayers, XRD θ–2θ scans were carried out, as demonstrated in figure 2. The peaks located around 34.46° ∼ 35.09° are attributed to the diffraction from $Be_xZn_{1-x}O$ (0 0 2) planes. When Be is alloyed into the hexagonal lattice of ZnO, the (0 0 2) diffraction peak is largely shifted from 34.46° (ZnO) to 34.91° ($Be_{0.06}Zn_{0.94}O$) and 35.09° ($Be_{0.1}Zn_{0.9}O$). It is quite reasonable because the plane distance along the (0 0 2) orientation is decreased due to the much smaller ionic radius of Be^{2+} (0.27 Å) than that of Zn^{2+} (0.60 Å). Note that a small peak appears at 41.66° in the $Be_{0.1}Zn_{0.9}O$ film, which is quite close to the position of the BeO (0 0 2) diffraction peak (41.40°). In view of the large lattice strain between ZnO and BeO, the new peak at 41.66° was attributed to the $Zn_xBe_{1-x}O$ in the BeO lattice. That means phase segregation emerges when the Be content increases to 10%. This finding has been rarely reported or discussed in previous literature.

It is imaginable that phase segregation will cause an undesirable influence on the bandgap engineering. The RS results prove that the bandgap values of the $Be_{0.06}Zn_{0.94}O$ and $Be_{0.1}Zn_{0.9}O$ films just shift a little from that of ZnO (figure 3). The strong band edge peaks were observed at 371.6 nm (3.34 eV) and 374.4 nm (3.31 eV) for $Be_{0.06}Zn_{0.94}O$ and $Be_{0.1}Zn_{0.9}O$, respectively. Compared to the value of

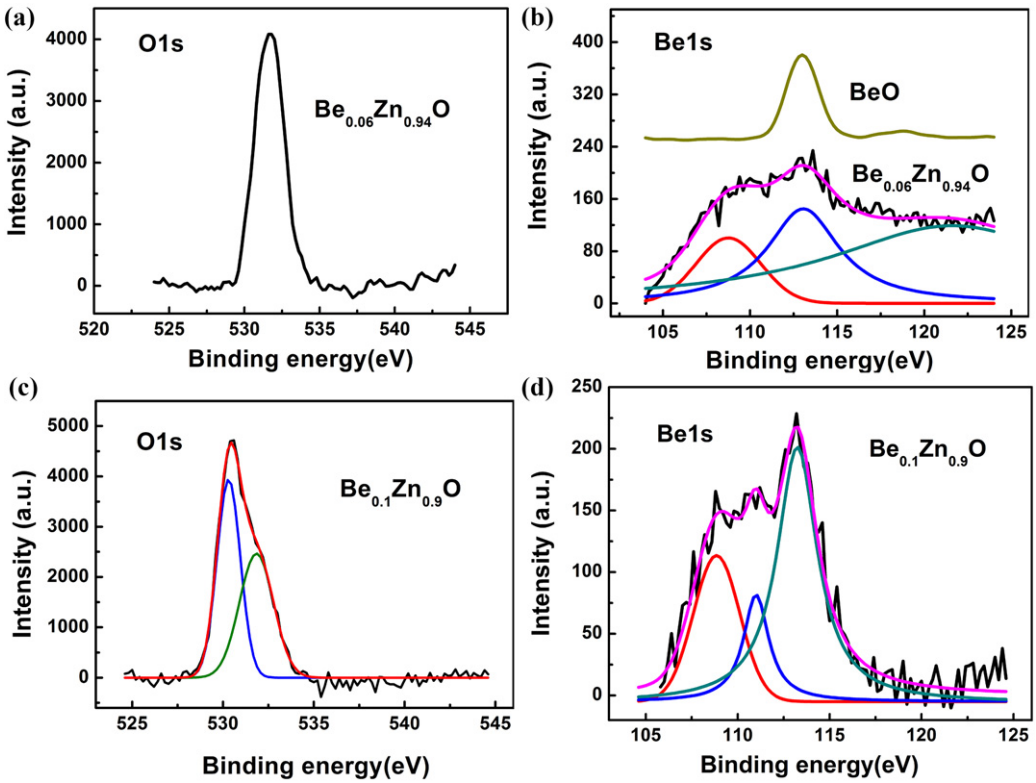

Figure 4. O 1s and Be 1s XPS spectra of $Be_{0.06}Zn_{0.94}O$ (*a*) and (*b*), of $Be_{0.1}Zn_{0.9}O$ (*c*) and (*d*).

375.3 nm (3.30 eV) for ZnO, the bandgap of $Be_{0.06}Zn_{0.94}O$ only shifts 40 meV and that of $Be_{0.1}Zn_{0.9}O$ only shifts 10 meV. Obviously, the efforts to modulate the bandgap of ZnO through Be alloying over a wide range of wavelength values failed, partly because of the observed phase segregation of $Zn_xBe_{1-x}O$.

The electrical properties of $Be_xZn_{1-x}O$ films were obtained by Van der Pauw Hall measurements, where the Hall voltage can be traced to determine the exact carrier conductivity type [15]. The ZnO sample shows normal electrical properties with carrier density $N = 4.66 \times 10^{17}\,\mathrm{cm}^{-3}$, mobility $\mu = 41\,\mathrm{cm\,V^{-1}\,s^{-1}}$ and resistivity $\rho = 0.326\,\Omega\,\mathrm{cm}$. The BeO film shows an insulating nature with a huge resistance that is difficult to test. The N, μ and ρ for $Be_{0.06}Zn_{0.94}O$ and $Be_{0.1}Zn_{0.9}O$ are calculated as 2×10^{18} and $1.02 \times 10^{18}\,\mathrm{cm}^{-3}$, 0.3 and $0.74\,\mathrm{cm\,V^{-1}\,s^{-1}}$, and $10\,\Omega\,\mathrm{cm}$ and $26\,\Omega\,\mathrm{cm}$, respectively. It should be noted that the Hall voltages of the $Be_{0.1}Zn_{0.9}O$ sample are very small and hence not as easy to be recognized as the ones in $Be_{0.06}Zn_{0.94}O$. So the electrical properties of $Be_{0.1}Zn_{0.9}O$ are not as accurate as those of $Be_{0.06}Zn_{0.94}O$. It is well known that accurate Hall data of Van der Pauw measurements can be obtained only on a uniform film. The abnormal Hall signals are supposed to originate from the different regional electrical properties, such as the low resistance area from interstitial Be clusters and the insulating area from BeO phase segregation. It is suggested that such a low-/high-resistance islands distribution in BeZnO films makes it difficult to achieve reliable p-type conductivity.

The formation of Be_i is another important factor for the hardly tuned band structure of $Be_{0.06}Zn_{0.94}O$ and $Be_{0.1}Zn_{0.9}O$. In order to verify the existence of Be_i, XPS measurements were carried out on these samples. Before the tests, all of the samples were sputtered by an Ar ion gun for 4 s, to remove the upper 1 nm contaminated surface layer. Shown in figure 4 are the O 1s and Be 1s core electron spectra of $Be_{0.06}Zn_{0.94}O$ and $Be_{0.1}Zn_{0.9}O$, respectively. Only O–Zn chemical bonding at 531.7 eV was found in $Be_{0.06}Zn_{0.94}O$ (figure 4(*a*)), while the Be 1s core electron associated with Be–O bonding (113.04 eV) can be clearly seen in figure 4(*b*), in good consistence with the result obtained from BeO film (113.0 eV). It indicates that some Be atoms are incorporated into the Zn sites in the ZnO lattice. In addition, the Be 1s core level of the Be atom exhibits an asymmetric shoulder centring at 108.77 eV. We speculate that this signal is originated from Be_i, although the binding energy is deviated from that of the metallic states of Be 1s [16]. The different chemical environment may be the main reason for the large shift in binding energy. This peak has also been mentioned in some Be–N co-doped ZnO samples [10, 11].

From the O 1s fitting curve of $Be_{0.1}Zn_{0.9}O$ (figure 4(*c*)), the O–Be bonding related peak appears at 530.29 eV, and the relative intensity of the Be–O peak (figure 4(*d*)) increases with the increase of the Be content from $x = 0.06$ to 0.1. Notably, these phenomena occur together with the phase segregation in $Be_{0.1}Zn_{0.9}O$ (shown in figure 2). Interestingly, the Be 1s curve can be fitted into three Gaussian components. The 108.8 eV and 113.2 eV are assigned to Be_i and Be–O, respectively. The middle peak between them is located at 111.05 eV and seems closer to the metallic Be 1s level. In terms of the interstitial nature of the Be atoms in our $Be_xZn_{1-x}O$ films, one possibility is the splitting of the Be_i 1s peak. Similar to the Al 2p electron spectrum in AlO_x-passivated metallic

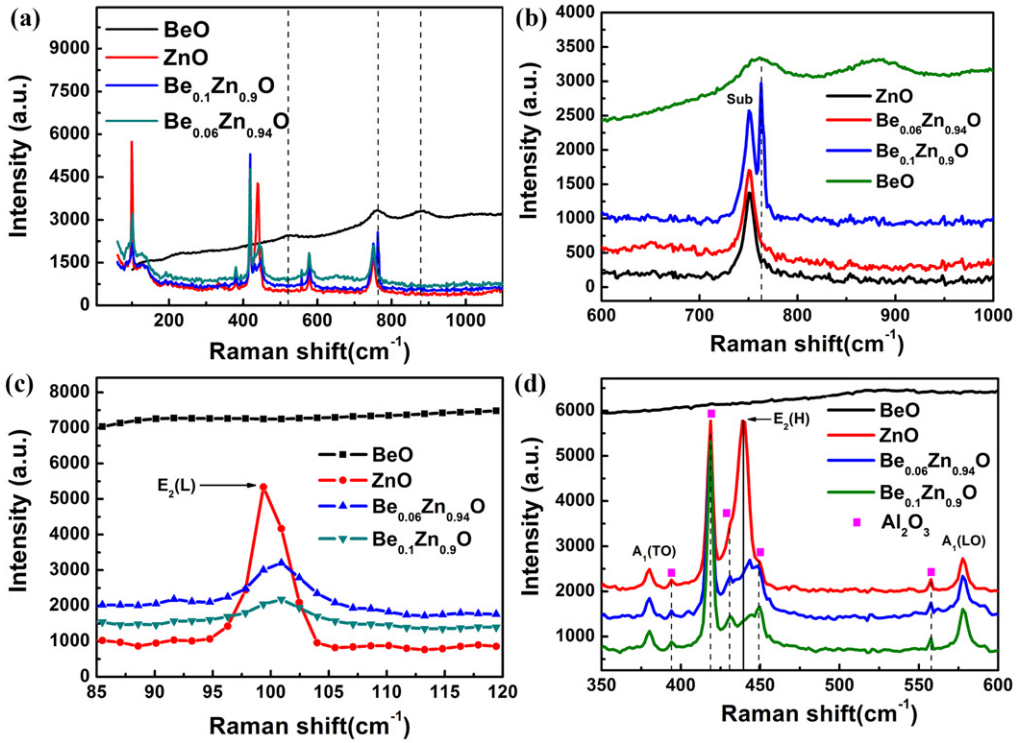

Figure 5. Raman spectra of ZnO, BeO, $Be_{0.06}Zn_{0.94}O$ and $Be_{0.1}Zn_{0.9}O$: (*a*) in the frequency range of 50–1100 cm^{-1}, and enlarged curves (*b*) in the frequency range of 600–1000 cm^{-1}, (*c*) in the frequency range of 85–120 cm^{-1}, and (*d*) in the frequency range of 350–600 cm^{-1}.

Al [17], a splitting peak will emerge in the larger binding energy side of the original Be 1s peak, when Be is coated or surrounded by BeO. Further studies need to be carried out to verify this assumption. It can be concluded from the XPS analysis that some Be atoms occupy Zn sites in the ZnO lattice while formation of Be_i inevitably occurs. Furthermore, BeO phase segregation appears in higher Be-content $Be_xZn_{1-x}O$ films. That is why $Be_{0.1}Zn_{0.9}O$ has a poorer crystal quality and a smaller bandgap energy.

To further prove our argument, Raman spectra (figure 5) measurements were carried out and studied at room temperature, with a 532 nm laser illuminating the samples' surface. Four normal modes of ZnO were observed at 99 cm^{-1}, 380 cm^{-1}, 437 cm^{-1} and 577 cm^{-1}, corresponding to E_2 (low), A_1 (TO), E_2 (high) and A_1 (LO), respectively (figure 5 (*a*)). Three new modes were identified at 523.14, 762.65 and 878.34 cm^{-1} in BeO, which were obviously different from the available experimental and theoretical data [18]. Such discrepancy mainly originates from the different lattice constants obtained by different growth methods. After comparing the Raman spectra of ZnO, BeO, $Be_{0.06}Zn_{0.94}O$ and $Be_{0.1}Zn_{0.9}O$ films, a new extra peak belonging to BeO emerges at 762.65 cm^{-1} in the $Be_{0.1}Zn_{0.9}O$ sample (figure 5(*b*)). It suggests that BeO phase separation exists in $Be_{0.1}Zn_{0.9}O$, which is consistent with the XRD and XPS results. It should be noted that the intensity of this peak is even stronger than the substrate signals, and it is also much sharper and narrower than its corresponding counterpart of BeO film. Taking into consideration the possibility of Be interstitial clusters coated or surrounded by BeO, the stronger and sharper signal may be the Be surface plasmon-enhanced Raman scattering of BeO.

In figures 5(*c*) and (*d*), both E_2 (low) and E_2 (high) peaks of ZnO were found to be broader and weaker with increased Be composition, with significant shifts to higher frequencies of 100.83 cm^{-1} and 443.77 cm^{-1}, respectively. Similar results have been observed in Li-doped ZnO, where substitutional and interstitial Li co-exist [19]. The change of both E_2 (low) and E_2 (high) modes indicates that the interstitial Be clusters and Be^{2+} ions in Zn^{2+} sites strongly affect the lattice integrity and crystallinity. The structural disorder breaks the symmetry of the host lattice, which leads to the peak broadening, weakening and shifting to higher frequencies.

In conclusion, the sites Be occupies in BeZnO alloy films are given by a comparative study. It is found that substitutional and interstitial Be atoms co-exist in $Be_{0.06}Zn_{0.94}O$, and phase-segregated $Zn_xBe_{1-x}O$ occurs when Be composition increases to 10%. On the other hand, the substitutional Be content decreases instead of increasing, which may be responsible for the difficulty of reliable p-type conductivity in Be–N co-doped ZnO.

Acknowledgments

This work was supported by the National Science Foundation (Grant nos 61076007, 11174348, 51272280, 11274366, 61204067), the Ministry of Science and Technology of China (Grant nos 2011CB302002, 2011CB302006), and the Chinese Academy of Sciences.

References

[1] Ryu Y R, Lubguban J A and Lee T S 2007 *Appl. Phys. Lett.* **90** 131115

[2] Ryu Y R, Lee T S, Lubguban J A, White H W, Kim B J, Park Y S and Youn C 2006 *Appl. Phys. Lett.* **88** 241108
[3] Yang C, Li X M, Gu Y F, Yu W D, Gao X D and Zhang Y W 2008 *Appl. Phys. Lett.* **93** 112114
[4] Wei M, Boutwell R C, Mares J W, Scheurer A and Schoenfeld W V 2011 *Appl. Phys. Lett.* **98** 261913
[5] Du X L, Mei Z X, Liu Z L, Guo Y, Zhang T C, Hou Y N, Zhang Z, Xue Q K and Kuznetsov A Yu 2009 *Adv. Mater.* **21** 4625
[6] Hou Y N, Mei Z X, Liu Z L, Zhang T C and Du X L 2011 *Appl. Phys. Lett.* **98** 103506
[7] Ryu Y R, Lee T S, Lubguban J A, Corman A B, White H W, Leem J H, Han M S, Park Y S, Youn C J and Kim W J 2006 *Appl. Phys. Lett.* **88** 052103
[8] Jeong T-S, Han M S, Kim J H, Baeand S-J and Youn C-J 2007 *J. Phys. D: Appl. Phys.* **40** 370
[9] Yamamoto T and Yoshida H K 1999 *Japan. J. Appl. Phys.* **38** L166
[10] Sanmyo M, Tomita Y and Kobayashi K 2003 *Chem. Mater.* **15** 819
[11] Sanmyo M, Tomita Y and Kobayashi K 2005 *Thin Solid Films* **472** 189
[12] Tang X, Deng Y Z, Wagner D, Yub L and Lue H F 2012 *Solid State Commun.* **152** 1
[13] He X, Gu L, Guo S D, Liu Z L, Yu R C, Mei Z X, Du X L, Liu B G, Ikuhara Y C and Duan X F 2013 *J. Phys. D: Appl. Phys.* **46** 145303
[14] Azarov A Y, Jensen J, Halle A and Aggerstam T 2008 *J. Appl. Phys.* **104** 053509
[15] Guo Y, Liu Y P, Li J Q, Zhang S L,Mei Z X and Du X L 2010 *Chin. Phys. Lett.* **27** 067203
[16] NIST X-ray Photoelectron Spectroscopy Database (http://srdata.nist.gov/xps/Default.aspx)
[17] Chang S L, Andegregg J W and Thiel P A 1996 *J. Non-Cryst. Solids* **195** 95
[18] Kourouklis G A, Sood A K and Hochheimer H D 1985 *Phys. Rev.* B **31** 8332
[19] Yadav H K, Sreenivas K, Gupta V and Katiyar R S 2008 *J. Appl. Phys.* **104** 053507